Available online at www.sciencedirect.com
SCIENCE DIRECT®
Bioorganic & Medicinal Chemistry Letters 15 (2005) 3771–3774
Bioorganic & Medicinal Chemistry Letters

Synthesis and structural modeling of the amphiphilic siderophore rhizobactin-1021 and its analogs

Evgeny A. Fadeev, Minkui Luo and John T. Groves*

Department of Chemistry, Princeton University, Princeton, NJ 08544, USA

Received 13 April 2005; revised 13 May 2005; accepted 16 May 2005
Available online 28 June 2005

Abstract—We describe two convenient syntheses of rhizobactin-1021 (**Rz**), a citrate-based siderophore amphiphile produced by the nitrogen-fixing root symbiont *Rhizobium meliloti-1021*, and several analogs. Our approach features a singly amidated, *tert*-butyl-protected citrate intermediate that easily affords a variety of **Rz** analogs in the late stages of the synthesis. Structural modeling and the monolayer behavior of **Rz** and its metal complexes are consistent with a structural reorganization upon **Rz**-mediated iron chelation.

The principal strategy for bacterial response to iron restriction is to secrete siderophores, a family of small organic compounds with a highly selective iron-chelating ability.[1] These microbial iron chelators have attracted attention not only due to their essential functions for bacterial growth[2] but also because of a variety of pharmacological applications.[3] Drug-conjugated siderophores have been described as potential Trojan Horse vehicles for antibiotic delivery;[4] siderophore-based iron scavengers have shown promising therapeutic activities for breast cancer,[5] reperfusion injury,[6] and malaria,[7] and siderophore-like chelators can be used for the treatment of iron-overload diseases.[8,9] Consequently, studies in these fields still largely depend on the availability of structurally diverse natural and artificial siderophores.

Rhizobactin-1021 (**Rz**) is a citrate-based siderophore amphiphile produced by the nitrogen-fixing root symbiont *Rhizobium meliloti-1021*.[10] A unique aspect of the **Rz** structure lies in its two non-equivalent hydroxamate subunits, with one long hydrocarbon chain (Fig. 1). We recently showed that the overall structures of siderophore amphiphiles play important roles in their membrane-interaction properties.[11–13] The α,β-unsaturated hydroxamate moiety in **Rz** is also found in acinetoferrin,[14] mycobactins,[2] and nannochelin A.[15] Accordingly, the structural features, biological properties, and

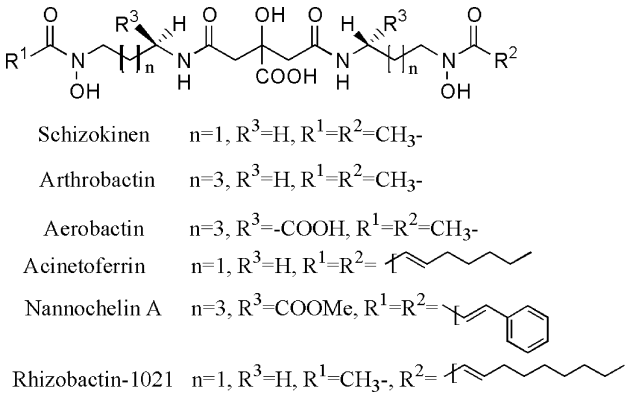

Figure 1. Structures of rhizobactin-1021 (**Rz**) and its analogs.

possible therapeutic applications of **Rz** stimulated us to develop a convenient access to this compound and its analogs.

In this paper, we describe two synthetic approaches to **Rz**. The overall unsymmetrical structure of **Rz** makes its synthesis more challenging than those of its symmetric counterparts.[11,15–22] The core strategy was to design an unsymmetrical precursor suitable for the preparation of various **Rz** analogs by a universal procedure. The molecular conformations and monolayer behavior of **Rz** and its metal complexes were also investigated.

Scheme 1 shows our two synthetic approaches to racemic **Rz** and its analogs. The key step for the first

Keywords: Amphiphile; Iron; Structure; Acinetoferrin; Mycobactin.
* Corresponding author. Tel.: +1 609 258 3593; fax: +1 609 258 0348; e-mail: jtgroves@princeton.edu

0960-894X/$ - see front matter © 2005 Elsevier Ltd. All rights reserved.
doi:10.1016/j.bmcl.2005.05.114

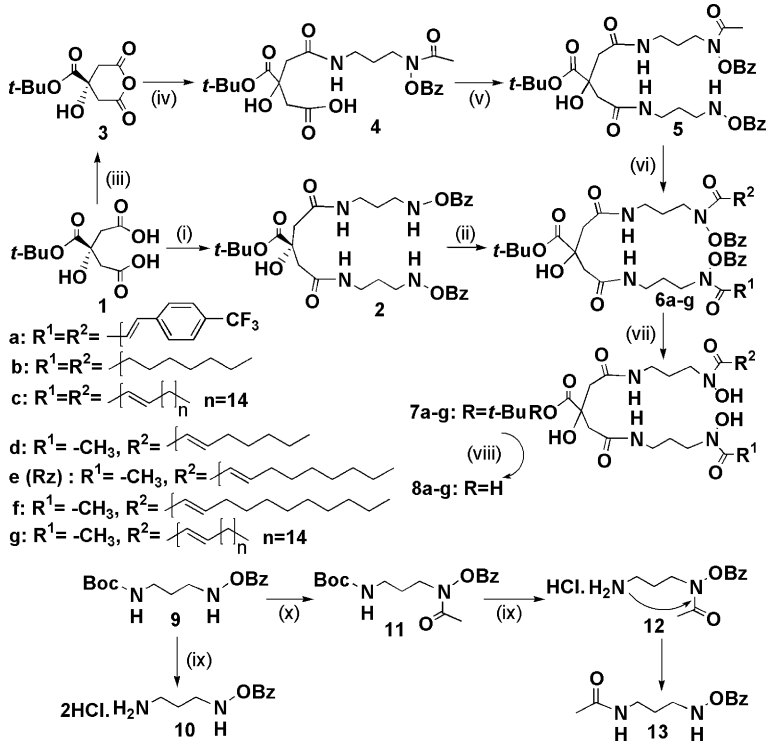

Scheme 1. Synthesis of the citrate-based amphiphilic siderophore rhizobactin-1021 (**Rz**) and its analogs. Reagents and conditions:[25] (i) a. DCC, HOSu/dioxane; b. **10** + TEA/CH_3CN; (ii) a. R^1COCl/DCM, −78 °C ($R^1 \neq R^2$); b. R^2COCl/DCM, reflux; (iii) DCC/DCM; (iv) **12**/DCM, 25 °C; (v) a. DCC, HOSu/DCM, 25 °C; b. **10** + TEA/DCM; (vi) R^2COCl/DCM (R^1=CH_3), reflux; (vii) 5 N NaOH/CH_3OH, 0 °C; (viii) TFA/H_2O, 19:1; (ix) HCl gas; (x) Acetyl chloride/DCM, reflux.

approach (**1** → **4** → **6**) is to differentiate the two carboxylic acid groups of the citrate moiety. This goal was accomplished via preparing the singly amidated citrate derivative (**4**) by coupling 1-*N*-(acetyl-benzoyloxy)-1,3-diaminopropane hydrochloride (**12**) with the *tert*-butyl-protected cyclic citric anhydride (**3**). This anhydride intermediate is readily obtained from the *tert*-butyl-protected citric acid (**1**)[20] via DCC-facilitated intramolecular dehydration in 90% yield. The amine hydrochloride (**12**) was synthesized via acetylation of *N*-(benzoyloxy)-3-(*tert*-butoxycarbonylamino)propyl-amine[22,23] and subsequent deprotection of the *tert*-butoxycarbonyl group with dry HCl (**9** → **12**, yield 96% and 82% for the two steps, respectively). This early installation of the acetyl hydroxamate moiety allows ready modifications for a variety of analogs (**8c–f**) simply by attaching different *trans*-2-alkenoyl chains (**6** → **7**). The hydrochloride salt was chosen for compound **12**, since the more typical procedure of using TFA afforded an oil and facilitated the undesirable acyl transfer reaction (**12** → **13**).[24] This rearrangement was further compensated by the use of 30% excess **12** in the subsequent coupling reaction (**3** → **4**). Here, the yield of **4** was quantitative with respect to **3**. Compound **4** was not easily separated from the acyl transfer byproduct **13** through column chromatography; however, compound **4** could be purified via repetitive washing using aqueous HCl (pH 2). This compound was then converted into the activated *N*-(hydroxyl)succinimidyl ester that underwent facile coupling with 1-*N*-benzoyloxy-1,3-diaminopropane dihydrochloride (**10**) to give compound **5**.[11] For the steps **3** → **5**, we found it unnecessary to pursue the rigorous purification of **4**, since compound **13** did not react under the subsequent conditions. Consequently, the first column purification could be postponed until the preparation of **5** with the overall yield of 51% (**3** → **5**). These *tert*-butyl-protected citrate intermediates completely avoid the undesirable imide formation via intramolecular condensation.[18,22,24] The fully protected precursors of **Rz** and its unsymmetrical analogs (**6d–g**) were obtained by coupling with the corresponding *trans*-2-alkenoyl chloride in 70%–80% yield. The deprotections of the benzoyl and *tert*-butyl groups (**6d–g** → **8d–g**) were carried out with aqueous NaOH/MeOH (80%–95%) and 95% TFA/water, respectively.[11] Consequently, compounds **8d–g** were obtained with an overall yield of 26%–35% with respect to **1**. The ^{1}H NMR spectrum of racemic compound **8e** (**Rz**) obtained in this way was identical to that of authentic rhizobactin-1021.[10]

We also synthesized racemic **Rz** via another more straightforward approach (**1** → **2** → **6e** in Scheme 1). Intermediate **2** was prepared as we have described by coupling *tert*-butyl-protected citric acid (**1**) with 1-*N*-benzoyloxy-1,3-diaminopropane dihydrochloride (**10**).[11] This symmetrical citrate diamide (**2**) was then reacted with one equivalent of *trans*-2-decenoyl chloride and then acetyl chloride. The resulting mixture consisted of a nearly statistical ratio of compound **6e** as the major component with the two expected symmetrical products. This target compound **6e** was readily purified by thin-layer chromatography. We found that the addition

of the less reactive *trans*-2-decenoyl chloride before the acetyl chloride maximized the yield of **6e**. We also noticed that running the first acylation reaction at −78 °C for 2 h gave the highest yield of the monoacyl-coupled intermediate. The second *N*-benzoyloxyamino moiety in **2** was then rapidly reacted with excess acetyl chloride in refluxing DCM to prevent further acylation by *trans*-2-decenoyl chloride. This one-pot reaction eventually gave an overall yield of 48% of **6e**. **Rz** (**8e**) was obtained through the same deprotection protocols as described above. Here, we also prepared **8a–c**, three symmetric analogs of **Rz**, by reacting **2** with the corresponding acyl chlorides (80% yield for **2** → **6a–c** and 80%–95% for **6a–c** → **8a–c**, 31%–36% overall from **2**).

The likely molecular conformations of **Rz** and its metal complex (Fig. 2) were derived from the NMR structures that we have reported for acinetoferrin (**Af**) and schizokinen.[11,12] All diastereomers of Fe-**Rz** adopt similar 3-D orientations except chirality. Similar to the symmetrical citrate siderophores,[11,12] the **Rz** iron complex has most of its polar residues buried inside and its hydrocarbon skeleton exposed to the outside. The negative charge of **Rz** metal complex is delocalized over the metal center and its six coordinating oxygens. This conformational change of Fe-**Rz** would be expected to facilitate its membrane flip-flop.[12] The N-*cis*-*cis* conformation of **Rz** metal complex makes its terminal methyl and *trans*-2-decenoyl chain adopt an anti-parallel orientation with the angle of 130°.[11] However, the overall structure of the **Rz** metal complex is much less extended than that of its **Af** analog, because of the short methyl group in the former vs the long octenoyl chain in the latter.

The headgroup sizes of **Rz** and its iron complex were measured via Langmuir–Blodgett techniques to further understand the conformational changes upon **Rz**-mediated iron chelation. As shown in Figure 3, **Rz** and Fe-**Rz** form well-behaved Langmuir monolayers. Headgroup sizes of 28 and 46 Å^2 were obtained for **Rz** and Fe-**Rz**, respectively, by extrapolating the solid-monolayer region to zero surface pressure. The 18 Å^2 increase of **Rz** headgroup size indicates that iron chelation causes a structural reorganization in **Rz**. The smaller headgroup size of Fe-**Rz** (46 Å^2) in contrast to the mean molecular area of Fe-**Af** (114 Å^2) is consistent with the N-*cis*-*cis*

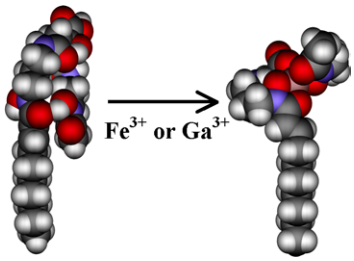

Figure 2. Likely 3-D structures of **Rz** and its metal complex (a representative 3-D structure). These structures were derived by analogy to acinetoferrin and its gallium complex.[11] There is a structural reorganization in the headgroup region of **Rz** upon iron chelation.

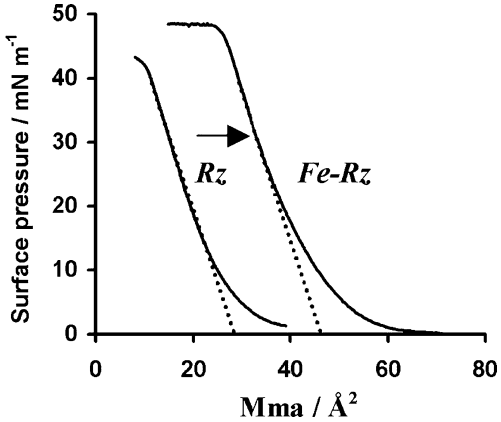

Figure 3. Measurements of mean molecular areas (Mma) using Langmuir–Blodgett techniques. The variations of the surface pressure were recorded by pressing the monolayers after a 30-min incubation of **Rz** onto the air/subphase interface (HEPES buffered solution, at pH 7.4 and 20 °C, in the presence and absence of 5 mM **FAC** for **Rz** and Fe-**Rz**, respectively). The headgroup sizes of **Rz** and Fe-**Rz** were obtained by extrapolating the linear region to zero surface pressure with Mma 28 Å^2 for **Rz** and 46 Å^2 for Fe-**Rz**, respectively.

coordination of Fe-**Rz** and Fe-**Af**.[11] In this coordination geometry the extended side chain orientation for Fe-**Af** would account for the 68 Å^2 increase relative to Fe-**Rz** due to the incommensurate arrangement of the second hydrocarbon chain with respect to the parallel packing of the phospholipid side chains.[11,12] The headgroup size of Fe-**Rz** (46 Å^2) reported here is in good agreement with the structural models of **Rz** metal complexes described above. As we have suggested, changes in headgroup size and molecular conformation upon binding iron are likely important determinants of membrane binding and permeability.[12]

This work reports the first synthesis of **Rz** (**8e**) and its unsymmetrical analogs (**8d** and **8f–g**). Each of the two approaches has its respective merits. The first one (**1** → **4** → **6**) provides ready access to a variety of **Rz**-based homologs via the common intermediate **5** without major change of the procedure. Furthermore, this strategy may be adopted for large-scale or combinatorial solid-phase synthesis and to prepare fluorophore-conjugated analogs by substituting the hydrocarbon moieties with hydrophobic fluorescent probes. Such derivatives are useful for siderophore-mediated intracellular trafficking studies. The second approach (**1** → **2** → **6**) provides a straightforward route to obtain a few hundred milligrams of compound in a short period of time. In addition, both approaches keep the iron-chelating moieties protected until the final stage and therefore minimize the iron contamination. Iron chelation by **Rz** causes an expansion of the size of the headgroup by 18 Å^2, consistent with the structural models of **Rz** and its metal complex. The molecular structures and monolayer properties of **Rz** and its metal complex further argue that this amphiphile can interact with biological membranes. Studies of iron acquisition and membrane behavior of **Rz** and its analogs are ongoing.

Acknowledgments

Support of this work by the National Science Foundation (CHE-0316301 and CHE-0221978) through the Environmental Molecular Science Institute (CEBIC) at Princeton University is gratefully acknowledged.

Supplementary data

Supplementary data associated with this article can be found in the online version at doi:10.1016/j.bmcl.2005.05.114.

References and notes

1. Albrecht-Gary, A. M.; Crumbliss, A. L. *Met. Ions Biol. Syst.* **1998**, *35*, 239.
2. Ratledge, C.; Dover, L. G. *Annu. Rev. Microbiol.* **2000**, *54*, 881.
3. Roosenberg, J. M.; Lin, Y. M.; Lu, Y.; Miller, M. J. *Curr. Med. Chem.* **2000**, *7*, 159.
4. Durham, T. B.; Miller, M. J. *J. Org. Chem.* **2003**, *68*, 27.
5. Pahl, P. M. B.; Horwitz, M. A.; Horwitz, K. B.; Horwitz, L. D. *Breast Cancer Res. Treat.* **2001**, *69*, 69.
6. Horwitz, L. D.; Sherman, N. A.; Kong, Y. N.; Pike, A. W.; Gobin, J.; Fennessey, P. V.; Horwitz, M. A. *Proc. Natl. Acad. Sci. U.S.A.* **1998**, *95*, 5263.
7. Golenser, J.; Tsafack, A.; Amichai, Y.; Libman, J.; Shanzer, A.; Cabantchik, Z. I. *Antimicrob. Agents Chemother.* **1995**, *39*, 61.
8. Turcot, I.; Stintzi, A.; Xu, J. D.; Raymond, K. N. *J. Biol. Inorg. Chem.* **2000**, *5*, 634.
9. Bergeron, R. J.; Wiegand, J.; McManis, J. S.; Bussenius, J.; Smith, R. E.; Weimar, W. R. *J. Med. Chem.* **2003**, *46*, 1470.
10. Persmark, M.; Pittman, P.; Buyer, J. S.; Schwyn, B.; Gill, P. R.; Neilands, J. B. *J. Am. Chem. Soc.* **1993**, *115*, 3950.
11. Fadeev, E. A.; Luo, M.; Groves, J. T. *J. Am. Chem. Soc.* **2004**, *126*, 12065.
12. Luo, M.; Fadeev, E. A.; Groves, J. T. *J. Am. Chem. Soc.* **2005**, *127*, 1726.
13. Xu, G. F.; Martinez, J. S.; Groves, J. T.; Butler, A. *J. Am. Chem. Soc.* **2002**, *124*, 13408.
14. Okujo, N.; Sakakibara, Y.; Yoshida, T.; Yamamoto, S. *Biometals* **1994**, *7*, 170.
15. Bergeron, R. J.; Phanstiel, O. *J. Org. Chem.* **1992**, *57*, 7140.
16. Bergeron, R. J.; Huang, G. F.; Smith, R. E.; Bharti, N.; McManis, J. S.; Butler, A. *Tetrahedron* **2003**, *59*, 2007.
17. Gardner, R. A.; Ghobrial, G.; Naser, S. A.; Phanstiel, O. *J. Med. Chem.* **2004**, *47*, 4933.
18. Guo, H. Y.; Naser, S. A.; Ghobrial, G.; Phanstiel, O. *J. Med. Chem.* **2002**, *45*, 2056.
19. Lee, B. H.; Miller, M. J. *J. Org. Chem.* **1983**, *48*, 24.
20. Milewska, M. J.; Chimiak, A.; Glowacki, Z. *J. Prakt. Chem.* **1987**, *329*, 447.
21. Miller, M. J.; Maurer, P. J. *J. Am. Chem. Soc.* **1982**, *104*, 3096.
22. Wang, Q. X. H.; Phanstiel, O. *J. Org. Chem.* **1998**, *63*, 1491.
23. Wang, Q. X. H.; King, J.; Phanstiel, O. *J. Org. Chem.* **1997**, *62*, 8104.
24. Ghosh, A.; Miller, M. J. *J. Org. Chem.* **1993**, *58*, 7652.
25. Compound **11**, ^{1}H NMR: (300 MHz, $CDCl_3$): δ 1.41 (s, 9H, CH_3), 1.79 (m, 2H, CH_2), 2.06 (s, 3H, $COCH_3$), 2.88 (t, 2H, BocN–CH_2), 3.21 (m, 2H, CON–CH_2), 5.08 (br s, 1H, NH), 7.54 (m, 2H, aromatic), 7.70 (m, 1H, aromatic), 8.11 (m, 2H, aromatic). Compound **12**, ^{1}H NMR (400 MHz, CD_3OD): δ 2.01 (q, 2H, CH_2), 2.08 (s, 3H, CH_3), 3.08 (t, 2H, N-CH_2), 3.96 (t, 2H, CON–CH_2), 7.60 (t, 2H, aromatic), 7.77 (t, 1H, aromatic), 8.14 (d, 2H, aromatic). Anal Calcd for $C_{12}H_{17}ClN_2O_3$: C, 52.85; H, 6.28; Cl, 13.00; N, 10.27, found: C, 52.94; H, 6.92; Cl, 14.55; N, 10.75. Compound **3**, ^{1}H NMR (400 MHz, $CDCl_3$): δ 1.48 (s, 9H, CH_3), 2.96 (q, 4H, CH_2). Anal Calcd for $C_{10}H_{14}O_6$: C, 52.17; H, 6.13, found: C, 52.22; H, 6.08. Compound **5**, ^{1}H NMR (400 MHz, $CDCl_3$): δ 1.41 (s, 9H, $3\times CH_3$), 1.77 (m, 4H, $2\times$ C–CH_2–C), 2.00 (s, 3H, $COCH_3$), 2.59 (m, 4H, $2\times COCH_2$), 3.15 (m, 2H, BzON–CH_2), 3.28 (m, 4H, $2\times$ CON–CH_2), 3.82 (m, 2H, CON(BzO)–CH_2), 6.86 (m, 1H, NH), 6.95 (m, 1H, NH), 7.44 (m, 4H, aromatic), 7.63 (m, 2H, aromatic), 7.95 (m, 2H, aromatic), 8.03 (m, 2H, aromatic). HRESIMS Calcd for $C_{32}H_{42}N_4O_{10} + Na^+$ 665.2799, found 665.2787. Anal Calcd for $C_{32}H_{42}N_4O_{10}$: C, 59.80; H, 6.59; N, 8.72, found: C, 59.35; H, 6.43; N, 8.49. Compound **6e**, ^{1}H NMR (400 MHz, CD_3OD): δ 0.86 (t, 3H, C_9–CH_3), 1.28 (m, 10H, $5\times$ –CH_2–), 1.44 (s, 9H, $3\times CH_3$), 1.88 (m, 4H, $2\times$ C–CH_2-C), 2.06 (br s, 3H, $COCH_3$), 2.18 (m, 2H, C=C–CH_2), 2.62 (ab-quartet, 4H, $2\times$ OC–CH_2), 3.28 (m, 4H, $2\times$ CON–CH_2), 3.90 (m, 4H, $2\times$ CON(BzO)–CH_2), 6.18 (d, 1H, OC-CH=), 6.98 (m, 1H, =CH–C), 7.62 (m, 4H, aromatic), 7.72 (m, 2H, aromatic), 7.95 (m, 4H, aromatic), 8.16 (m, 4H, aromatic). HRESIMS Calcd for $C_{42}H_{58}N_4O_{11} + Na^+$ 817.4000, found 817.3976. Compound **8b**. ^{1}H NMR (400 MHz, $CDCl_3$): δ 0.82 (t, 6H, C_7–CH_3), 1.24 (m, 16H, $8\times$ –CH_2–), 1.51 (m, 4H, $2\times$ CO–C–CH_2), 1.71 (m, 4H, $2\times$ C–CH_2–C), 2.37 (m, 4H, $2\times$ N(BzO)–CO–CH_2–), 2.60 (ab-quartet, 4H, $2\times$ OC–CH_2), 3.10 (m, 4H, $2\times$ CON–CH_2), 3.56 (m, 4H, $2\times$ CON(BzO)–CH_2). ^{13}C NMR (400 MHz, CD_3OD): δ 14.16, 23.83, 26.12, 27.72, 30.35, 30.35, 30.65, 33.08, 33.46, 37.81, 45.21, 46.89, 75.23, 172.27, 176.46, 177.01. HRESIMS Calcd for $C_{28}H_{52}N_4O_9 + Na^+$ 611.3632, found 611.3626. Compound **8e**, ^{1}H NMR (400 MHz, CD_3OD): δ 0.83 (t, 3H, C_9–CH_3), 1.34 (m, 8H, $4\times$ –CH_2–), 1.42 (m, 2H, C=C–C–CH_2), 1.76 (m, 4H, $2\times$ C–CH_2–C), 2.02 (s, 3H, $COCH_3$), 2.16 (m, 2H, C=C–CH_2), 2.60 (ab-quartet, 4H, $2\times COCH_2$), 3.12 (m, 4H, $2\times$ CON–CH_2), 3.60 (m, 4H, $2\times$ CON(O)–CH_2), 6.52 (d, 1H, COCH=), 6.76 (m, 1H, =CH–). HRESIMS Calcd for $C_{24}H_{42}N_4O_9 + H^+$ 531.3030, found 531.3021.